Chlorine in wadsleyite and ringwoodite: An experimental study

Mathilde Roberge, Hélène Bureau, Nathalie Bolfan-Casanova, Caroline Raepsaet, Suzy Surble, Hicham Khodja, Anne-Line Auzende, Patrick Cordier, Guillaume Fiquet

Chlorine in wadsleyite and ringwoodite: an experimental study

Mathilde Roberge[1], Hélène Bureau[1], Nathalie Bolfan-Casanova[2], Caroline Raepsaet[3], Suzy Surble[3], Hicham Khodja[3], Anne-Line Auzende[4], Patrick Cordier[5], Guillaume Fiquet[1].

[1] Institut de Minéralogie, de Physique des Matériaux et de Cosmochimie (IMPMC), Sorbonne Universités – UPMC Univ. Paris 06, CNRS UMR 7590, Muséum National d'Histoire Naturelle, IRD UR 206, 4 place Jussieu, 75252 Paris Cedex 05, France

[2] Laboratoire Magmas et Volcans, Université Blaise Pascal, Clermont-Ferrand, France

[3] LEEL, NIMBE, CEA, CNRS, Université Paris-Saclay, CEA Saclay, 91191 Gif-sur-Yvette Cedex, France

[4] Université Grenoble Alpes, ISTerre, UMR5275 F-38041 Grenoble cedex 9, France

[5] UMET Lille

For submission to *Earth and Planetary Sciences Letters*

Keywords: Chlorine, transition zone, experimental study, volatiles

Corresponding author : Hélène Bureau

e-mail : helene.bureau@impmc.upmc.fr

Abstract

We report concentrations of Chlorine (Cl) in synthetic wadsleyite (Wd) and ringwoodite (Rw) in the system NaCl-$(Mg,Fe)_2SiO_4$ under hydrous and anhydrous conditions. Multi-anvil press experiments were performed under pressures (14-22 GPa) and temperatures (1100-1400°C) relevant to the transition zone (TZ: 410-670 km depth). Cl and H contents were measured using Particle Induced X-ray Emission (PIXE) and Elastic Recoil Detection Analysis (ERDA) respectively. Results show that Cl content in Rw and Wd is significantly higher than in other nominally anhydrous minerals from the upper mantle (olivine, pyroxene, garnet), with up to 490 ppm Cl in anhydrous Rw, and from 174 to 200 ppm Cl in hydrous Wd and up to 113 ppm Cl in hydrous Rw.

These results put constrains on the Cl budget of the deep Earth. Based on these results, we propose that the TZ may be a major repository for major halogen elements in the mantle, where Cl may be concentrated together with H_2O and F (see Roberge et al., 2015). Assuming a continuous supply by subduction and a water-rich TZ, we use the concentrations measured in Wd (174 ppm Cl) and in Rw (106 ppm Cl) and we obtain a maximum value for the Cl budget for the bulk silicate Earth (BSE) of $15.1x10^{22}$ g Cl, equivalent to 37 ppm Cl. This value is larger than the 17 ppm Cl proposed previously by McDonough and Sun (1995) and evidences that the Cl content of the mantle may be higher than previously thought. Comparison of the present results with the budget calculated for F (Roberge et al., 2015) shows that while both elements abundances are probably underestimated for the bulk silicate Earth, their relative abundances are preserved. The BSE is too rich in F with respect to heavy halogen elements to be compatible with a primordial origin from chondrites CI-like (carbonaceous chondrites CC) material only. We thus propose a combination of two processes to explain these relative abundances: a primordial contribution of different chondritic-like materials, including EC-like (enstatite chondrites), possibly followed by a distinct fractionation of F during the Earth differentiation due to its lithophile behaviour compared to Cl, Br and I.

1. Introduction

Halogen elements (fluorine F, chlorine Cl, bromine Br, iodine I) are minor volatiles compared to hydrogen and carbon. Major halogens F and Cl have been mostly studied for their role in the shallowest Earth's reservoirs: lithosphere, crust, atmosphere, and hydrosphere, mostly because they are the most abundant halogens and because they have been shown to be strongly involved in volcanic and igneous processes. Indeed, Cl is an important constituent of volcanic fumaroles and plumes, and form individualized fluids such as brines and molten salts. These brines are strongly involved in hydrothermal systems and in ore forming processes (see the reviews after Pyle and Mather 2009; Shinohara 2009; Aiuppa et al., 2009). Cl is particularly used to trace igneous processes and ore-forming processes, and to track magmas from their genesis to their eruption Cl is known to affect magma properties (see Pyle and Mather, 2009), it is significantly degassed from subaerial volcanic activity (e.g. Aiuppa, 2009), and it can impact the stratosphere chemistry. Cl is enriched in sea water, it has been shown that oceanic subduction delivers fluids to the mantle through serpentinites related processes (serpentinization and deserpentinization), that are significantly Cl-rich (e.g. Ito et al., 1983; John et al., 2011; Kendrick et al., 2011), making this last one an important constituent in mantle metasomatism processes, that enriches the sources for arc magmatism (e.g. Tatsumi, 1989, Philippot et al., 1998; Scambelluri et al., 2004). Indeed magmas from subduction zones are among the most enriched in Cl (Ito et al., 1983; Straub and Layne, 2003; Kendrick et al., 2012).

During subduction, the interaction between seawater and rocks produces secondary minerals containing significant amounts of Cl (Ito et al., 1983; Pagé et al., 2016). It has thus been proposed that the subduction of oceanic lithospheric material at convergent plate boundaries would drive an annual global flux of 2.9-22 x 10^{12} g Cl to the Earth's interior (John et al., 2011). It has also been proposed that a part of the subducted Cl would reach high depths in the mantle (>200 km) and would possibly enrich the sources for Ocean Island Basalts (Kendrick et al., 2015; Joachim et al., 2015). Cl is significantly present in ultrahigh pressure metamorphic rocks (Scambelluri et al., 2004; Ottolini and Fèvre, 2008; Pagé et al., 2016), in kimberlites (Kamenetsky et al., 2004), and in inclusions of saline brines in diamonds (Weiss et al., 2014). Recent studies show that Cl is present in olivine, pyroxene, and garnet: the highest contents of Cl are measured in minerals formed by metamorphic dehydration of serpentine, olivines and pyroxenes (up to 400 ppm Cl, Scambelluri et al., 2004; Ottolini and Fèvre, 2008). In natural upper mantle nominally anhydrous minerals, the Cl contents are very low: up to 6.3 ppm in olivine (Beyer et al., 2012). Partitioning experiments performed for natural compositions however demonstrate the capability of upper mantle minerals to be the Cl carriers: up to 148 ppm Cl in orthopyroxene, 17 ppm Cl in clinopyroxene, 13 ppm in garnet, 5 ppm in plagioclase, up to 170 ppm in olivine (Dalou et al., 2012). To our knowledge, there is currently no evidence about the presence of Cl in the transition zone and in the lower mantle. Recently we have suggested that a strong link connects the water global cycle and that of fluorine at depth (Crepisson et al., 2014; Roberge et al., 2015). We have proposed that the transition zone can be a major reservoir for fluorine (Roberge et al., 2015). It could be similar for Cl.

This study aims at constraining the possible deep storage and cycling of Cl through the determination of Cl potential contents in wadsleyite (Wd) and ringwoodite (Rw), the major minerals of the transition zone (TZ). We use these data to discuss the Cl content of the bulk silicate Earth.

2. Materials and methods

2.1. Starting materials an experimental strategy

The starting bulk composition was olivine Fo_{90} with a slight excess of silica ((Mg+Fe)/Si atomic ratio =1.75), obtained with a mixture of (1) oxide powders of MgO, SiO_2, FeO, or (2) natural Fo_{90} olivine with SiO_2 powder. 5 wt% of Cl was added to the mixture as crushed NaCl powder. NaCl was chosen as the source of Cl because it is enriched in sea water and in subducted oceanic floor. For experiments under hydrous conditions, 2wt% of water was added as brucite $Mg(OH)_2$, an amount close to the expected water solubility in wadsleyite and ringwoodite in the transition zone. Samples were synthesized in multi-anvil presses at LMV Clermont-Ferrand (France) and at the Bayerisches Geoinstitut of Bayreuth (Germany) following the procedure described in Frost et al. (2001) and Demouchy et al. (2005). Experiments were performed from 14 to 22 GPa and from 1100°C to 1400°C during 0.5 to 9 hours, (Table 1). The samples were enclosed in Re, Pt or Au-Pd capsules. Temperatures were monitored with W3Re/W25Re thermocouples located at the top of the capsules. After the run, the experiments were quenched by switching off the electric power before decompression.

2.2. Sample characterization

The mineral assemblages were recovered, embedded in epoxy and mirror polished on one side. They were analyzed with Raman spectroscopy and scanning electron microscopy at first. The textures were investigated with a Zeiss Ultra 55 field emission scanning electron microscope (SEM) equipped with an Energy Dispersive X-Ray spectroscopy (EDX) system. Major elements compositions of wadsleyites and ringwoodites were subsequently measured by Electron Probe Micro Analysis (EPMA) on CAMECA-SX100 at CAMPARIS facility (UPMC, France). For these quantitative analyses, we used an acceleration voltage of 15 kV and a beam current of 10 nA with an 15 µm defocused beam.

A thin section of ringwoodite sample was prepared with a Focus Ion Beam (FIB), using a gallium beam with a FEI Strata DB 235 at IEMN (Lille France). A transmission Electron Microscopy (TEM) study was performed on this FIB section at UMET, Lille (France) with a FEI Tecnai G2-20 twin operating at 200 kV.

Chlorine and hydrogen contents were measured using ion beam analysis, Particle Induced X-Ray Emission (PIXE) for Cl and Elastic Recoil Detection Analysis (ERDA) for H at the nuclear microprobe of the Laboratoire d'Etude des Eléments Légers (LEEL), CEA Saclay. Cl concentrations of the mineral phases Wd and Rw were obtained using incident beams of 3*3 μm^2 mapped on large areas (50*50 to 200*20 μm^2). The procedure is detailed in (Bureau et al., 2010; 2015). We used different incident beams (H^+ and $^4He^+$ from 1.7 to 3 MeV) in order to control the depth of investigation in the samples. With mineral phases a few tens of µm in size embedded in a quenched Cl-Si-rich glass (present at grain boundaries), compromise had to be found between energy and detection in order to avoid any chlorine contribution from glassy phase. Indeed the depths investigated by the ion beams depend both on the nature of the incident ion (H^+, $^4He^+$) and on the energy of the beam, (*i.e.* the highest the energy is the deepest is the investigation). For a San Carlos olivine, the depth of analysis for a proton beam is 50 µm at 3 MeV and 25 µm at 1.7 MeV. For one given energy, this depth is reduced when the incident ion is heavier than H^+, at 2 MeV the investigated depth of $^4He^+$ is 6 µm.

Hydrogen (i.e. water) contents of Rw and Wd were measured using ERDA. We used a 3 MeV $^4He^+$ beam, following the protocol described in Raepsaet et al. (2008), Bureau et al. (2009) and Withers et al. (2012). Simultaneous Cl analysis were also performed by PIXE during ERDA.

We scanned the beam on selected areas of the sample (from 30x30 to 150x100 μm^2). Durations of analysis were chosen from 1800 to 7200 seconds. ERDA and PIXE were associated to simultaneous Rutherford Backscattering Spectrometry (RBS) measurements used to monitor the cumulated charge delivered to the sample during the acquisition (see Bureau et al., 2009). They also provided information on the matrix chemical composition of the samples. For all ion beam analysis, the software RISMIN (Daudin et al., 2003) was used to process the data by selecting the areas of interest in the chemical maps (see Fig. 1). It was particularly useful for the detection of NaCl-rich glasses (grain boundaries, cracks or surface contamination), which would affect H and Cl contents. Once the areas were selected, ERDA spectra were processed by using SIMNRA (Mayer et al., 1997) and PIXE spectra were processed by using the GUPIXWIN software (Campbell et al., 2000). Analysis were cross-checked against: NIST SRM610 glass (Rocholl et al., 1997), KE12 (pantellerite lava from Kenya, Metrich and Rutherford, 1992), EtC3 (Cl-Br-I-bearing $NaAlSi_3O_8$ glass, Bureau et al., 2000). The sensitivity (i.e. detection limit) with respect to Cl was of a few tens of ppm (30-40 at maximum) depending on the conditions (beam energy, grain size, size of the selected areas).

3. Results

3.1. Synthesized samples

Ten samples were synthesized (see Table 1). Among these samples, two are volatile-free (no H_2O and no Cl), two are anhydrous (Cl-enriched but no H_2O), and six are Cl-H_2O-enriched. Recovered mineralogical assemblages are described in Table 1. They correspond to the mineral assemblages expected for the pressure and temperature conditions of the transition zone. The minerals are in equilibrium with a saline and silica-rich melts mostly present at grain boundaries. SEM shows that wadsleyite and ringwoodite phases exhibit subhedral or euhedral shapes and various crystal sizes (Fig. 1 and 2). In the runs performed at 14 GPa, we observe enstatite in agreement with literature (Inoue 1994; Inoue et al. 1995; Bolfan-Casanova 2000). For runs performed at 22 GPa, stishovite (∼10 μm in size) is found in equilibrium with ringwoodite (50-300 μm in size Fig. 2). For all experiments, crystals are embedded in a Si-Na-Cl-rich interstitial glass at grain boundaries which corresponds to the residual melt. No particular textural differences or abrupt increase in the relative proportion amount of quenched glasses are noted between experiments performed at different temperatures. Optical observation and SEM measurements show that the crystals are pure, inclusion-free ringwoodites and wadsleyites (no visible inclusions). Furthermore, a 100 nm thickness lamella of ringwoodite (sample #S5553) was studied by transmission electron microscopy TEM (Figure 3). No Cl-rich or NaCl-rich micro or nano-inclusions have been observed.

EMPA analyses show that the Cl-bearing wadsleyites and ringwoodites exhibit a Mg# ratio (Mg#=Mg/(Mg+Fe) atomic ratio) ranging from 0.90 to 0.92 (Table 1 and 2), similar to the Earth's mantle mineral assemblage.

3.2. **Chemical Characterization**

PIXE and ERDA mapping of large areas of the samples show that there is no chemical zoning with respect to Cl and H in the Rw and Wd crystals. About 5 to 20 % in volume of NaCl-rich glasses are present in grain boundaries (Fig. 1). Enstatite is present at 5-10% volume in all the samples containing wadsleyite and stishovite is present at about 5-15% volume in all the samples containing ringwoodite. A comparison between the different Cl contents obtained from each analytical conditions (3 and 1.7 MeV, H^+ and He^+ beams) shows that detection limits and uncertainties for Cl are dependent on the energy and ion source used (Table 2). The analyses performed with a 3 MeV proton beam are the most sensitive to Cl contents but also to potential contamination (Cl-rich glasses located at grain boundary) because the depth of investigation is of about 50 µm. This depth is reduced to 25 µm for a beam of 1.7 MeV, and to a few µm for a ^4He+ beam of 3 MeV, but these two last conditions are much less sensitive. As the Cl contents determined at 3 MeV were systematically higher than the measurements performed at 1.7 MeV with a beam of H^+ or at 2 MeV with a beam of $^4He^+$, we have only considered the measurements performed at 1.7 MeV with a beam of H^+ and at 2 and 3 MeV with a beam of $^4He^+$. The lowest Cl content analysed was of 60 ppm, a value higher than the detection limit. Two samples could not be analysed for Cl due to the very small size of the crystals.

Results show that Cl contents are significant, and range from 60 ± 60 to 200 ± 48ppm Cl for Wd and from 99 ± 12 to 490 ±33 ppm Cl for Rw. Anhydrous Rw contain more Cl than hydrous Rw, with a maximum of 490 ppm Cl. Unfortunately, we failed analysing Cl in anhydrous Wd because crystals were too small. Cl contents of hydrous Wd are ranging from 60 ± 60 to 200 ± 48 ppm Cl with corresponding water contents ranging from 917 ± 15 to 1659 ± 14 ppm H_2O. Cl contents of hydrous Rw are ranging from 99 ± 12 to 490 ±33 ppm Cl for water contents from 932 ± 14 to 4766 ± 13 ppm H_2O.

No relationship is observed between the temperature and both Cl and H_2O contents (i.e. OH contents expressed as water equivalent concentrations, see Fig. 4 and 5). A slight decrease of Cl content with pressure may be suggested for hydrous samples. The incorporation of Cl in anhydrous Rw is higher than in hydrous Rw (Fig. 4 and 5). No significant dependency is found between the Cl content and Mg#, FeO, SiO_2 or (Mg+Fe)/Si atomic ratio.

The water contents determined in Wd and Rw from this study (from 917 to 4766 ppm wt. H_2O) are about one order of magnitude lower than the previously observed solubility values from the literature (Bolfan-Casanova et al., 2000, Inoue et al., 1995, Demouchy et al., 2005) that reached 3 to 2.2 wt. % respectively, at similar temperatures. In regard to the low Cl concentrations, we may exclude a competition between OH^- and Cl^- to enter in Wd and Rw structures. The significant reduction of OH incorporation cannot be compensated by an exchange between OH^- and Cl^-. Similar low water contents have been found in NaF-doped wadsleyite and ringwoodite (Roberge et al., 2015). One sample: #40_Cl, has been synthesized together with sample #40_F from this previous study. This suggests that the same process could lower water content in Rw and Wd for both F and Cl-bearing samples.

We propose the sodium salts NaCl as NaF to be responsible of this behaviour (see Roberge et al., 2015). A coupled incorporation mechanism of Na^+ and H^+ in both F and Cl-rich Wd and Rw may be responsible of the low water content rather than a competitive effect between halogen elements and hydroxyl groups (Roberge et al., 2015). Stalder et al. (2008) have reported a strong decrease of hydrogen incorporation in pure synthetic enstatite at 2.5 GPa, 1150-1400°C, and shown to be a function of the NaCl added in the starting materials. The low concentration of OH in enstatite is explained by a reduction of water activity in the fluid phase (melt or aqueous fluid) due to the presence of dissolved salt. In our experiments, the low water and possibly Cl content of the samples may be due to partitioning reaction between Rw and Wd and the Si-water and NaCl-rich melt (up to 20% in volume) in equilibrium with the minerals during the experiments. If true, the Cl concentrations cannot be considered as solubilities. It would also explain why the water contents are so low (4766 ppm wt% at maximum) compared to the initial amount of water (about 2 wt.%). Additional partitioning experiments involving a Mg-rich peridotitic melt would be necessary to validate this hypothesis. As a first assumption, we will consider that the Cl contents measured in Wd and Rw are corresponding to the maximum contents expected in Wd and Rw in a transition zone where interstitial melt may be present (e.g. Toffelmier et Tyburczy, 2007; Schmandt et al. 2014).

3.3 Cl versus F in ringwoodite and wadsleyite

A comparison between Cl contents (this study) and comparable F contents in Rw and Wd (Roberge et al., 2015) at conditions relevant to the transition zone is presented in figure 6. All the samples are comparable as we have used alternatively NaF or NaCl salts as starting materials, and the same pressure and temperature conditions. We observe that Cl contents are lower than F contents by a factor of 3 in anhydrous ringwoodites. For hydrous Rw and Wd it is more variable, as Cl contents are ranging from 60 ± 60 to 200 ± 48 ppm when F contents vary from 186 ± 19 to 850 ± 85 ppm. The difference between F and Cl solubility's in such chemical systems may reflect the difference in ionic size between F^- and Cl^-. It is likely F and OH share the same sites in olivine (Ol), wadsleyite and ringwoodite (Crepisson et al., 2014; Roberge et al., 2015), but this seems more unlikely for Cl which is larger than F and OH (Cl^- 181 nm, OH^- 140 nm). Fluorine incorporation in Ol, Wd, Rd is shown to be related to water incorporation (Crépisson et al., 2014, Roberge et al., 2015), but this is unclear for Cl. Indeed, similar Cl contents are observed in two samples of Rw with different water contents (Fig. 4). Further studies (i.e. FTIR spectroscopy) would be necessary to investigate into this direction. It is difficult to determine where Cl is incorporated in the crystal structure. The presence of OH defects in wadsleyite (Wd) and ringwoodite (Rw) have been investigated by coupling experimental observations to the modelling of infrared spectra (e.g, Blanchard et al. 2009; Blanchard et al., 2013) and provided insights into the crystal chemistry of OH in these minerals. The incorporation of Cl in Rw and Wd could be indirectly determined by studying the spectral signature of hydroxyl defects in NAMs, as for F-bearing hydrous olivines (Crépisson et al., 2014). As a first hypothesis, we suggest that in Wd and Rw, Cl, F and OH may occupy similar sites in the lattice, possibly mostly in association with Mg vacancies (as shown by Blanchard et al., 2013).

To summarize our major results: (1) the concentration of Cl in Wd and Rw is significant and can amount 490 ppm; (2) the concentration of Cl in Wd and Rw is 3 times smaller than compared to the concentration of F in the same phases synthesized in similar conditions; (3) anhydrous Rw are richer in both Cl and F than hydrous Rw; (4) the presence of water is not a pre-requisite to store Cl and F in these minerals. When present, water content is small, Cl and F contents may not be considered as solubility values for Wd and Rw, but would rather reflect partitioning reactions with an interstitial melt.

4. Discussion

4.1 Cl storage in the mantle Transition Zone's wadsleyite and ringwoodite phases

It is now recognized that the TZ is hydrated at least locally as shown by recent studies: (1) the significant water content of a hydrous ringwoodite trapped in a natural diamond exhumed from the transition zone (Pearson et al., 2014), (2) geophysical data (e.g. Huang et al., 2005). We consider hydrous Wd and Rw in the following sections: according to our measurements, ringwoodite contains 60 ± 60 ppm Cl and 917±15 ppm H_2O; wadsleyite can take up to 200 ± 48 ppm Cl and 1115±14 ppm H_2O. Such significant amounts are not surprising if we compare with the incorporation of fluorine in Wd and Rw (665 to 1045 ppm F, up to 956 ppm H_2O in Wd and 186 to 1235 ppm F, up to 1404 ppm H_2O in Rw, see Roberge et al., 2015). Furthermore, the range of water contents measured in Cl-rich Rw and Wd are consistent with what is predicted for the transition zone i.e. 1000-2000 ppm (Huang et al., 2005) and 2000 ppm – 2 wt.% (Bercovici and Karato, 2003).

We assume, that no significant amounts of Cl are dissolved in the other minor mineral phases of the TZ. We use an average pyrolitic composition with modal abundances of 60%wt. wadsleyite from 410 to 520 km and 60%wt. ringwoodite from 520 to 660 km with addition of 40%wt. of garnet and clinopyroxene from 410 to 660 km (Ringwood, 1975), and with the Cl contents of hydrous Fo90 wadsleyite and ringwoodite (174 ppm and 106 ppm respectively). An upper bound for Cl storage in the transition zone would be of $3x10^{22}$g Cl, corresponding to 80 ppm Cl. Wd and the Rw could be major carriers of the deep Cl, and should be thus taken into account for the Earth budget of this element.

In order to explain a chemical contrast between low water contents in the upper mantle with about 142 ppm water (Saal et al., 2002) and assuming a water-rich transition zone (having 0.2-2% wt% water), Bercovici and Karato (2003) have proposed the transition zone water-filter model. In this model, the downwelling fluxes driven by slabs into the transition zone and deeper lower mantle trigger a passive upwelling flow. At 410 km, this upwelling flow would rises out of the high-water-solubility transition zone with the transition of Wd to olivine together with a water release, as olivine has a lower solubility with respect to water than Wd (Bolfan-Casanova et al., 2000). Such a phase transition would then favour the formation of a melt layer overlying the transition zone, having a density higher than the solid phase. This layer would act as a filter, and would maintain a chemical contrast for trace and volatile elements between a depleted upper mantle and an enriched upper transition zone (Bercovici and Karato, 2003), it would permit a significant storage of Cl, F and H_2O in the transition zone.

4.2 How much Cl in the Bulk Silicate Earth?

Based on the average Cl contents in Mid Ocean Ridge Basalts, McDonough and Sun (1995) have estimated an abundance of 17 ppm Cl for the bulk silicate Earth. We have calculated the maximum Cl storage of the bulk silicate Earth, by adding the Cl contribution for each reservoir. Results are summarized in the figure 7, for Cl (this study) and for F (Roberge et al., 2015).

For the shallow reservoirs we assume the Cl crust contribution (ocean, evaporite, brine and crustal rock abundances) to be $5.8x10^{22}$ g (Sharp et al., 2013); we have used the value of 1 ppm Cl from Saal et al., (2002) to represent the depleted shallow upper mantle. For the transition zone, we assumed a hydrous TZ enriched in Cl, due to a continuous supply by subduction, we obtained a maximum storage of $3x10^{22}$ g of Cl, corresponding to the average concentration of 80 ppm. For the lower mantle we used the value of 21 ppm Cl calculated from Ocean Island Basalts compositions by Kovalenko et al. (2006), assumed to be representative of the primitive mantle. The resulting Bulk silicate Earth content for chlorine would then be of $15x10^{22}$ g, corresponding to a value of 37 ppm Cl, with a contribution of 20% from the transition zone (Figure 7). No significant change of the F/Cl ratio is observed (0.68, McDonough and Sun, 1995, 0.62, this study).

This estimate of 37 ppm Cl in the bulk silicate Earth is twice the previous one of 17 ppm (McDonough and Sun, 1995), it shows that the Earth's budget of Cl and F could be largely underestimated.

4.5 What about the origin of chlorine and fluorine of the Earth?

The origin of the volatile elements for the Earth is still highly debated today, but most of the models (e.g. Albarède, 2009; Javoy et al., 2010; Marty et al., 2012) propose that they originated from a cosmochemical reservoir that also sourced the parent bodies of primitive meteorites. The absence of correct condensation temperatures (Lodders, 2003) for both Cl and F makes difficult the calculation of the predicted abundances for Cl and F in an Earth accreted from any chondritic materials. For water, a chondritic origin is preferred because the terrestrial and chondritic D/H ratios are similar (see Marty and Yokochi, 2006 and references therein). Among the primitive meteorites, carbonaceous chondrites CC are the most popular candidates to reflect the Earth's volatile source. Marty (2012) shows that a later contribution of 2±1% of carbonaceous chondrite from the CI species to a dry proto-Earth would be consistent with the Earth atmophile elements (C, H, N, noble gases) and is in agreement with heavy halogen elements (Cl, Br, I) contents determined by McDonough and Sun (1995). However, according to Marty (2012), a contribution of 17% of CI would be necessary to explain the F abundance from McDonough and Sun (1995). A greater halogen content such as the one presented here cannot be easily reconciled with an Earth only built by homogeneous accretion of CI carbonaceous chondrite material. Alternatively, enstatite chondrites (EC) are F-enriched (i.e. F/Cl = 2.77 to 1.16, Rubin and Choi, 2009), with a heavy halogen element content similar to those of CI (Rubin and Choi, 2009). EC were already proposed to be the building material for the Earth (e.g. Javoy, 1995), based on the isotopic signature of oxygen and nitrogen. However, EC are water-poor, the Earth's Si isotopic compositions cannot be explained from a core-formation scenario from a BSE having a EC's composition, and the Mg/Si ratio of the upper mantle differs too much from the EC's. It is also proposed that the Earth was built from the mixing of a number of chondritic like end-members having different volatile compositions (Marty and Yokochi, 2006), including EC. The mixing of different volatile-rich late veneers is however not sufficient to explain the depletion of Cl (and also Br and I) compared to F of the BSE, which may reflect processes that have occurred during differentiation, after volatile acquisition (primitive or from a late veneer). Fluorine has a lithophile character compared to Cl, Br, I (McDonough and Sun, 1995). F content is greater than Cl content in both Wd and Rw. During the magma ocean crystallization, F could have been stored in mantle minerals whereas the heavier halogen elements may have been partially lost from the magma by devolatilization, a loss possibly due to their hydrophilic affinity (Sharp and Draper, 2013; Bureau et al., 2015). As long as the actual Cl and F budget of the Earth will remain un-determined, the origin of volatile elements of the Earth will remain an open question.

CONCLUSION

The experimental determination of the Cl concentration in hydrous wadsleyite and ringwoodite shows that they can be major carriers for Cl in the deep Earth. The transition zone can thus be a deep significant repository for Cl. Cl contents are lower by a factor of 3 than those observed by Roberge et al. (2015) for F. For both Cl and F, the presence of water lowers their concentrations in Rw and Wd, but this storage capacity remains significant. It is thus likely that both halogen elements are stored with water in the Earth's transition zone with a maximum content of 80 ppm Cl.

Nominally anhydrous minerals are the main Cl carriers in the mantle at least down to 660 km depth. Although it has been shown that F is strongly associated to water through incorporation mechanisms in the NAMs, Cl incorporation in silicate minerals lattice is not so clear and would deserve to be further studied. Assuming a continuous supply from subduction recycling, we calculate a maximum BSE content for chlorine of $15x10^{22}$ g Cl, corresponding to 37 ppm Cl is proposed. The corresponding global budget for Cl is twice the value proposed by McDonough and Sun (1995). In the light of these experimental results for both Cl and F, we propose that the modern relative abundances of Cl and F may result from the combination of two processes during the Earth's accretion: a mixing contribution of CC and EC chondritic-like materials (required to generate the F enrichment compared to Cl, Br, I); possibly followed by a fractionation of F from other halogen elements during the Earth's differentiation, whereas most of the F being stored in mantle minerals when part of the heavy halogens would have been preferentially partitioned in the magma ocean, degassed and lost.

Acknowledgments

We acknowledge Daniel J. Frost and the BGI's Staff, particularly H. Schulze, for their constant availability and precious help with the high pressure experiments performed in Bayreuth. We also thank the LMV's staff for their help during the experiments carried out in Clermont Ferrand. We are grateful to H. Khodja and the the LEEL staff during the analysis of the samples using the nuclear microprobe. We warmly thank J. C. Boulliard from the mineralogical collection of UPMC, I. Estève for her assistance during SEM analysis, O. Beyssac for access to the Raman spectrometer; and CAMPARIS staff for EMPA analyses.

We acknowledge John P. Brodholt, Editor for Earth and Planetary Sciences Letters, who has handled the manuscript. The manuscript was improved thanks to the detailed reviews of two anonymous reviewers.

The SEM of IMPMC which is supported by Région Ile de France Grant SESAME 2006 NOI-07-593/R, INSU-CNRS, INP-CNRS, UPMC, and by the French National Research Agency (ANR) Grant ANR-07-BLAN-0124-01. The FIB facility was supported by the French RENATECH network, and the TEM national facility in Lille (France) was supported by the Conseil Regional du Nord-Pas de Calais, the European Regional Development Fund (ERDF), and the Institut National des Sciences de l'Univers (INSU, CNRS). The national high-pressure facility multi-anvil presses, MLV Clermont-Ferrand, is also supported by INSU, CNRS. The present study was funded by the EGIDE PHC PROCOPE project 26673WC to H.B. and DAAD PROCOPE project 54366326 to D.J.Frost.

REFERENCES

Aiuppa, A., Baker, D.R., and Webster, J.D. (2009). Halogens in volcanic systems. Chem. Geol. *263*, 1–18.

Albarède F. (2009) Volatile accretion history of the terrestrial planets and dynamic implications, Nature, vol. 461, no 7268, p. 1227-1233.

Bercovici, D., and Karato, S. (2003). Whole-mantle convection and the transition-zone water filter. Nature *425*, 39–44.

Beyer, C., Klemme, S., Wiedenbeck, M., Stracke, A., and Vollmer, C. (2012). Fluorine in nominally fluorine-free mantle minerals: Experimental partitioning of F between olivine, orthopyroxene and silicate melts with implications for magmatic processes. Earth Planet. Sci. Lett. *337–338*, 1–9.

Blanchard, M., Balan, E., and Wright, K. (2009). Incorporation of water in iron-free ringwoodite: A first-principles study. Am. Mineral. *94*, 83–89.

Blanchard, M., Roberge, M., Balan, E., Fiquet, G., and Bureau, H. (2013). Infrared signatures of OH-defects in wadsleyite: A first-principles study. Am. Mineral. *98*, 2132–2143.

Bolfan-Casanova, N., Keppler, H., and Rubie, D.C. (2000). Water partitioning between nominally anhydrous minerals in the MgO–SiO2–H2O system up to 24 GPa: implications for the distribution of water in the Earth's mantle. Earth Planet. Sci. Lett. *182*, 209–221.

Bureau, H., Keppler, H., Métrich, N. (2000) Volcanic degassing of bromine and iodine : experimental fluid/melt partitioning data and applications to stratospheric chemistry, Earth and Planetary Science Letters, 183, 51-60.

Bureau, H., Raepsaet, C., Khodja, H., Carraro, A., and Aubaud, C. (2009). Determination of hydrogen content in geological. samples using elastic recoil detection analysis (ERDA). Geochim. Cosmochim. Acta *73*, 3311–3322.

Bureau, H., Auzende, A.-L., Marocchi, M., Raepsaet, C., Munsch, P., Testemale, D., Mézouar, M., Kubsky, S., Carrière, M., Ricolleau, A., Fiquet, G. (2015) The Volcanic degassing of Iodine, Geochimica et Cosmochimica Acta, 173, 114-125.

Campbell, J.L., Hopman, T.L., Maxwell, J.A., and Nejedly, Z. (2000). The Guelph PIXE software package III: Alternative proton database. Nucl. Instrum. Methods Phys. Res. Sect. B Beam Interact. Mater. At. *170*, 193–204.

Crépisson, C., Blanchard, M., Bureau, H., Sanloup, C., Withers, A.C., Khodja, H., Surblé, S., Raepsaet, C., Béneut, K., Leroy, C., et al. (2014). Clumped fluoride-hydroxyl defects in forsterite: Implications for the upper-mantle. Earth Planet. Sci. Lett. *390*, 287–295.

Dalou, C., Koga, K.T., Shimizu, N., Boulon, J., and Devidal, J.-L. (2012). Experimental determination of F and Cl partitioning between lherzolite and basaltic melt. Contrib. Mineral. Petrol. *163*, 591–609.

Daudin, L., Khodja, H., and Gallien, J.-P. (2003). Development of “position–charge–time” tagged spectrometry for ion beam microanalysis. Nucl. Instrum. Methods Phys. Res. Sect. B Beam Interact. Mater. At. *210*, 153–158.

Demouchy, S., Deloule, E., Frost, D.J., and Keppler, H. (2005). Pressure and temperature-dependence of water solubility in Fe-free wadsleyite. Am. Mineral. *90*, 1084–1091.

Frost, D.J., Langenhorst, F., van Aken, P.A. (2001). Fe-Mg partitioning between ringwoodite and magnesiowüstite and the effect of pressure, temperature and oxygen fugacity. Phys. Chem. Minerals 28, 455-470.

Huang, X., Xu, Y., and Karato, S. (2005). Water content in the transition zone from electrical conductivity of wadsleyite and ringwoodite. Nature *434*, 746–749.

Ito, E., Harris, D.M., and Anderson Jr., A.T. (1983). Alteration of oceanic crust and geologic cycling of chlorine and water. Geochim. Cosmochim. Acta *47*, 1613–1624.

Javoy, M. (1995). The integral enstatite chondrite model of the Earth. Geophys. Res. Lett. *22*, 2219–2222.

Joachim, B., Pawley, A., Lyon, I.C., Marquardt, K., Henkel, T. Clay, P.L., Ruzié, L., Burgess, R., Ballentine, C.J. (2015) Experimental partitioning of F and Cl between olivine, orthopyroxene and silicate melt at Earth's mantle conditions. Chem. Geol. 416, 65-78.

John, T., Scambelluri, M., Frische, M., Barnes, J.D., and Bach, W. (2011). Dehydration of subducting serpentinite: Implications for halogen mobility in subduction zones and the deep halogen cycle. Earth Planet. Sci. Lett. *308*, 65–76.

Kendrick, M.A., Scambelluri, M., Honda, M., Phillips, D. (2011) High abundances of noble gas and chlorine delivered to the mantle by serpentinite subduction. Nat. Geosci. 4, 807-812.

Kendrick, M.A., Woodhead, J.D., and Kamenetsky, V.S. (2012). Tracking halogens through the subduction cycle. Geology *40*, 1075–1078.

Kendrick, M.A., Jackson, M.G., Hauri, E.H., Phillips (2015). The halogen (F, Cl, Br, I) and H_2O systematics of Samoan lavas: Assimilated-seawater, EM2 and high- $^3He/^4He$ components. Earth and Planet. Sci. Lett. 410, 197-209.

Kovalenko, V.I., Naumov, V.B., Girnis, A.V., Dorofeeva, V.A., and Yarmolyuk, V.V. (2006). Composition and chemical structure of oceanic mantle plumes. Petrology *14*, 452–476.

Marty, B., Yokochi, R., (2006). Water in the Early Earth. Reviews in Mineralogy and Geochemistry 62, 421-450.

Marty, B. (2012). The origins and concentrations of water, carbon, nitrogen and noble gases on Earth. Earth Planet. Sci. Lett. *313-314*, 56–66.

Mayer, M., 1997. SIMNRA User's Guide. Report IPP 9/113, Max-Planck-Institut für Plasmaphysik, Garching, Germany.

McDonough, W.F., and Sun, S. -s. (1995). The composition of the Earth. Chem. Geol. *120*, 223–253.

Metrich, N., and Rutherford, M. (1992). Experimental-Study of Chlorine Behavior in Hydrous Silicic Melts. Geochim. Cosmochim. Acta *56*, 607–616.

Ottolini, L.P., and Fèvre, B.L. (2008). SIMS analysis of chlorine in metasomatised upper-mantle rocks. Microchim. Acta *161*, 329–336.

Pagé, L., Hattori, K., de Hoog, J.C.M., Okay, A.I. (2016). Halogen (F, Cl, Br, I) bahaviour in subducting slabs: a study in lawsonite blueshist in Western Turkey. Earth and Planet. Sci. Let. 442, 133-142.

Pearson, D.G., Brenker, F.E., Nestola, F., McNeill, J., Nasdala, L., Hutchison, M.T., Matveev, S., Mather, K., Silversmit, G., Schmitz, S., et al. (2014). Hydrous mantle transition zone indicated by ringwoodite included within diamond. Nature *507*, 221–224.

Philippot, P., Agrinier, P., and Scambelluri, M. (1998). Chlorine cycling during subduction of altered oceanic crust. Earth Planet. Sci. Lett. *161*, 33–44.

Pyle D. M. and Mather T. A., 2009. Halogens in igneous processes and their fluxes to the atmosphere and oceans from volcanic activity: A review, Chem. Geol., vol. 263, n° 1-4, p. 110-121.

Ringwood, A.E. (1975). Composition and Petrology of the Earth’s Mantle. McGraw-Hill *New York*.

Roberge, M., Bureau, H., Bolfan-Casanova, N., Frost, D.J., Raepsaet, C., Surblé, S., Khodja, H., Auzende, A.L. , Fiquet, G. (2015). Is the the transition zone a deep reservoir for fluorine? Earth and planet. Sci. Lett. 429, 25-32.

Rocholl, A.B.E., Simon, K., Jochum, K.P., Bruhn, F., Gehann, R., Kramar, U., Luecke, W., Molzahn, M., Pernicka, E., Seufert, M., et al. (1997). Chemical Characterisation of NIST Silicate Glass Certified Reference Material SRM 610 by ICP-MS, TIMS, LIMS, SSMS, INAA, AAS and PIXE. Geostand. Newsl. *21*, 101–114.

Rudnick R.L., Gao S. (2003). Composition of the continental crust. Treatrise on Geochemistry 3: 1-64.

Rubin, A.E., and Choi, B.-G. (2009). Origin of Halogens and Nitrogen in Enstatite Chondrites. Earth Moon Planets *105*, 41–53.

Saal, A.E., Hauri, E.H., Langmuir, C.H., and Perfit, M.R. (2002). Vapour undersaturation in primitive mid-ocean-ridge basalt and the volatile content of Earth’s upper mantle. Nature *419*, 451–455.

Scambelluri, M., Müntener, O., Ottolini, L., Pettke, T.T., and Vannucci, R. (2004). The fate of B, Cl and Li in the subducted oceanic mantle and in the antigorite breakdown fluids. Earth Planet. Sci. Lett. *222*, 217–234.

Sharp, Z.D., Draper, D.S. (2013) The Chlorine abundance of the Earth: Implications for a habitable planet. Earth and Planet. Sci. Lett. 369, 71-77.

Schmandt, B., S. D., Jacobsen, T. W., Becker, Z. X., Liu, K. G,. Dueker, 2014. Dehydration melting at the top of the lower mantle. Science, 344, 1265-1268.

Stalder, R., Kronz, A., and Simon, K. (2008). Hydrogen incorporation in enstatite in the system MgO–SiO_2–H_2O–NaCl. Contrib. Mineral. Petrol. *156*, 653–659.

Straub, S.M., and Layne, G.D. (2003). The systematics of chlorine, fluorine, and water in Izu arc front volcanic rocks: Implications for volatile recycling in subduction zones. Geochim. Cosmochim. Acta *67*, 4179–4203.

Tatsumi Y. (1989). Migration of fluid phases and genesis of basalt magmas in subduction zones. J. Geophys. Res. 94, 4697-4707.

Toffelmier, D.A., and Tyburczy, J.A. (2007). Electromagnetic detection of a 410-km-deep melt layer in the southwestern United States. Nature, 447, 991-994.

Weiss Y., Kiflawi I., Davies N., Navon O. (2014), High-density fluids and the growth of monocrystalline diamonds. *Geochimica et Cosmochimica Acta* 141, 145-159.

Withers, A.C., Bureau, H., Raepsaet, C., and Hirschmann, M.M. (2012). Calibration of infrared spectroscopy by elastic recoil detection analysis of H in synthetic olivine. Chem. Geol. *334*, 92–98.

Figure captions

Figure 1:

Sample #S5553 (1100°C and 20 GPa): hydrous Cl-bearing ringwoodite synthesized at 1100°C and 20 GPa.

A. PIXE spectrum of one Rw crystal Cl and Fe Kalpha and Kbeta rays respectively at 2.62 – 2.81 and 6.40 – 7.05 KeV are labelled on the spectrum.

B. SEM photography of sample #S5553. Ringwoodite (in light grey), the largest grain sizes are of more than 70 µm; stishovite is not present on this section, a Cl-rich melt is visible in grain boundaries. The white square is corresponding to the total map analysed with PIXE.

C. PIXE elemental map for iron.

D. PIXE elemental map for Cl.

A pure ringwoodite crystal is selected using the combination of the SEM photography with the elemental compositions (e.g. iron C and chlorine D) in order to avoid any chemical contamination from intersticial melt. This crystal is represented by the black shape in the SEM photography, and by the white shape in the chemical maps C and D. This area of interest (one ringwoodite crystal) is used to generate the PIXE spectrum presented in A.

Figure 2:

SEM photography of A) S5551 (anhydrous Cl-bearing ringwoodite synthesized at 1100°C and 20 GPa). Rw ringwoodite (in light grey), the grain sizes are of about 15 µm; St stishovite crystals are in dark grey with 6 µm medium size, intergranular glass is dark B) H3697 (hydrous Cl-bearing ringwoodite synthesized at 1400°C and 22 GPa), Rw ringwoodite (in light grey), the grain sizes are of about 20 µm; St stishovite crystals are in dark grey, intergranular glass is dark.

Figure 3

TEM analysis of a ringwoodite thin section of about 100 nm thickness (prepared by focused ion beam) for transmission electron microscopy study, from sample #S5553 (20 GPa, 1100°C, 240 min.) containing 99 ppm wt. Cl and 4766 ppm wt. H_2O.

A: Scanning Transmission Electron Microscopy (STEM) bright field micrograph of the ringwoodite showing the only heterogeneities found in the sample.

B and C: EDX analysis of Na and Cl contents within the green rectangle in A (1800 x 1100 nm^2), they show that heterogeneities are not related to any Cl-rich or NaCl-rich inclusions, and emphasize the uniform distribution.

Figure 4:

Cl content in ppm wt. versus temperature in °C. No significant effect of the temperature on the Cl content is seen.

Legend: white squares: hydrous wadsleyite, white triangles: hydrous ringwoodite. black triangle: anhydrous ringwoodite.

Figure 5:

Cl content in ppm wt. versus water contents in ppm wt. The highest Cl concentration is corresponding to anhydrous ringwoodite. Cl content seems to slightly decrease with water content, but we notice that for a same Cl content of about 100 ppm wt., the water content is ranging from 932 to 4766 ppm in ringwoodite. It would mean that the Cl content is not affected by water for such low amounts.

Same legend than Fig 4.

Figure 6:

Cl and F concentrations measured in Wd and Rw, synthesized using the same experimental protocol and from NaCl and NaF sources. Data from this study and from Roberge et al. (2015). Assuming a hydrous transition zone, ranges of potential Cl and F concentrations in Ol, Wd, Rw are proposed.

Legend: white squares: hydrous wadsleyite, white triangles: hydrous ringwoodite, white circles: olivines, black triangles: anhydrous ringwoodite, black square: anhydrous wadsleyite.

Figure 7

State of the art of the Cl and F budgets of the Earth, assuming a continuous supply by subduction of the TZ with respect to Cl and F. Reservoirs: crust (Rudnick and Gao, 2003); upper mantle without TZ (Saal, 2002); TZ, Cl this study, F (Rogerge et al., 2015); lower mantle, Cl (Beyer et al., 2012), F (Kovalenko et al., 2006). Degassing Fluxes are expressed in HCl (4.3 10^{12} g/yr) and HF (0.5 10^{12} g/yr), they are corresponding to 4.18 10^{12} g/yr Cl and 0.47 10^{12} g/yr F respectively, data are from Pyle and Mather (2009); subducted fluxes are from Straub and Layne (2003) and John et al. (2011).

Figure 1:

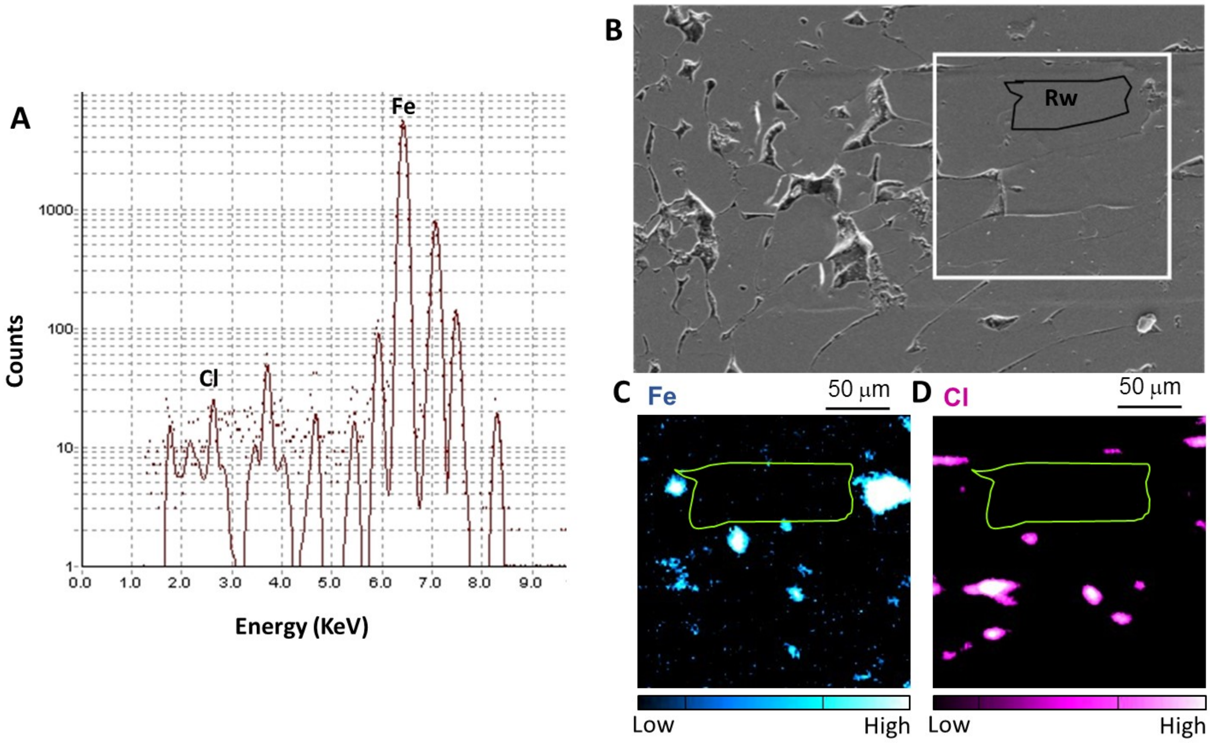
A
Fe
Cl
Counts
Energy (KeV)
B
Rw
C
Fe
50 µm
D
Cl
50 µm
Low
High
Low
High

Figure 2:

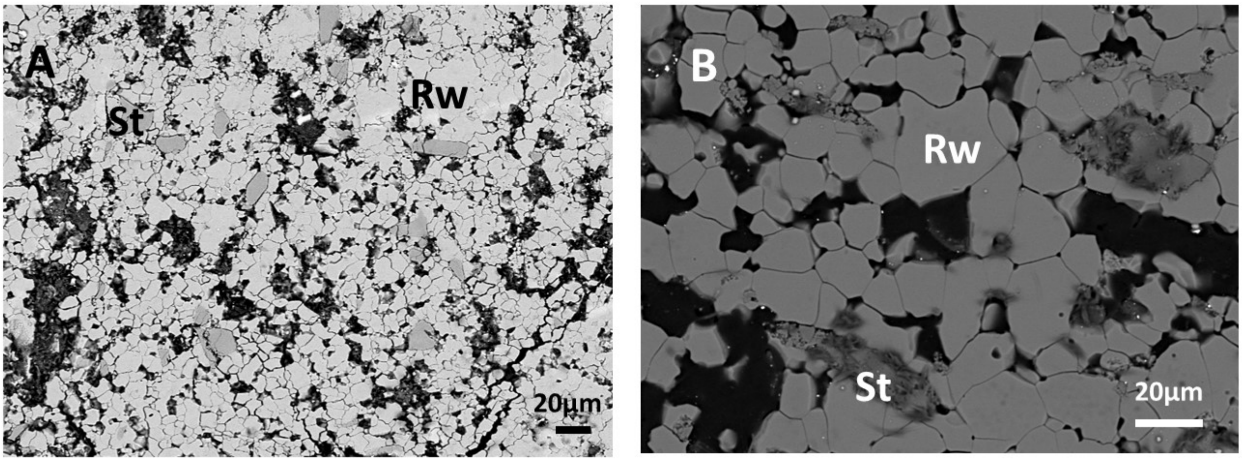

Figure 3:

Figure 4:

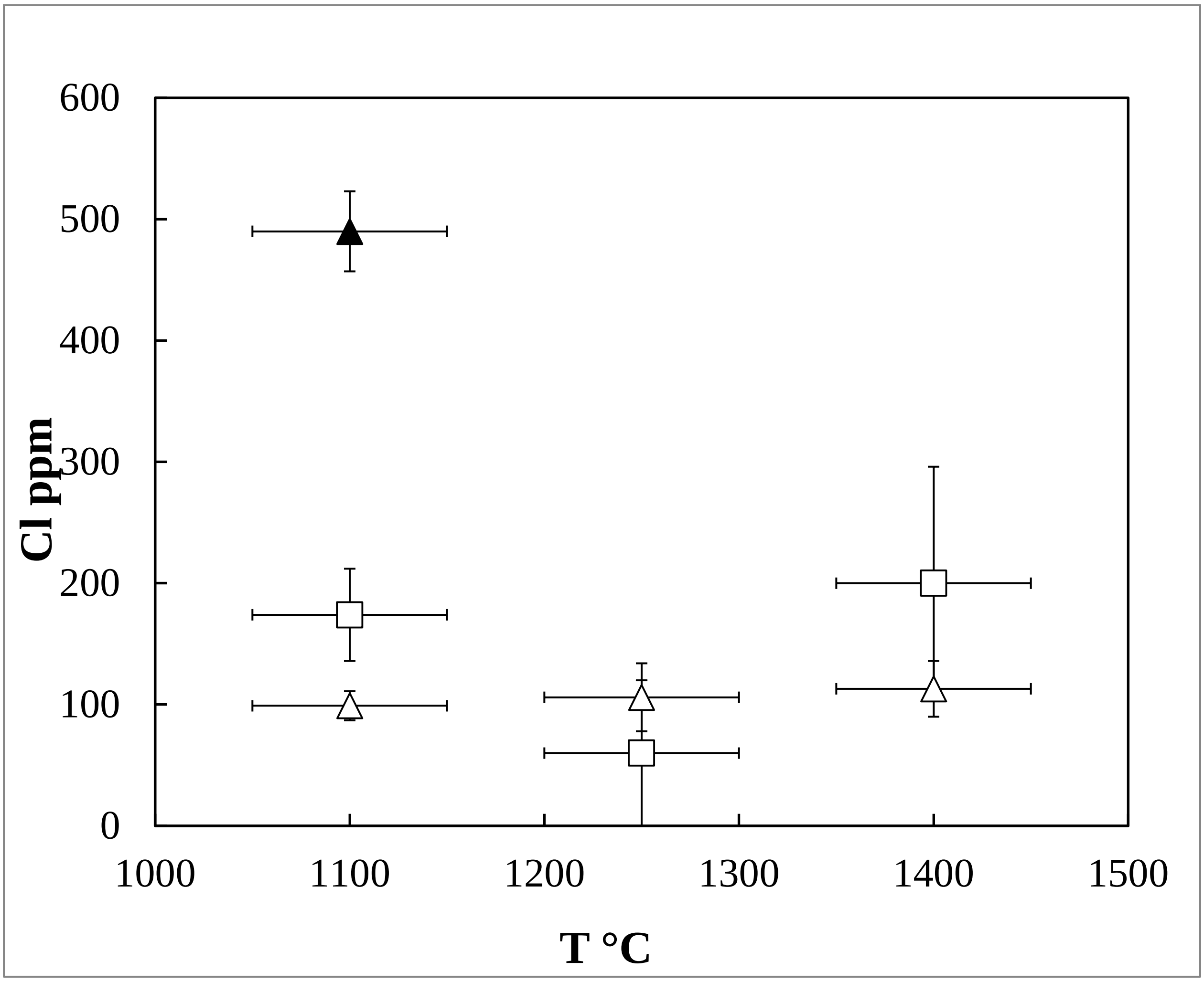
Cl ppm
0
100
200
300
400
500
600
1000
1100
1200
1300
1400
1500
T °C

Figure 5:

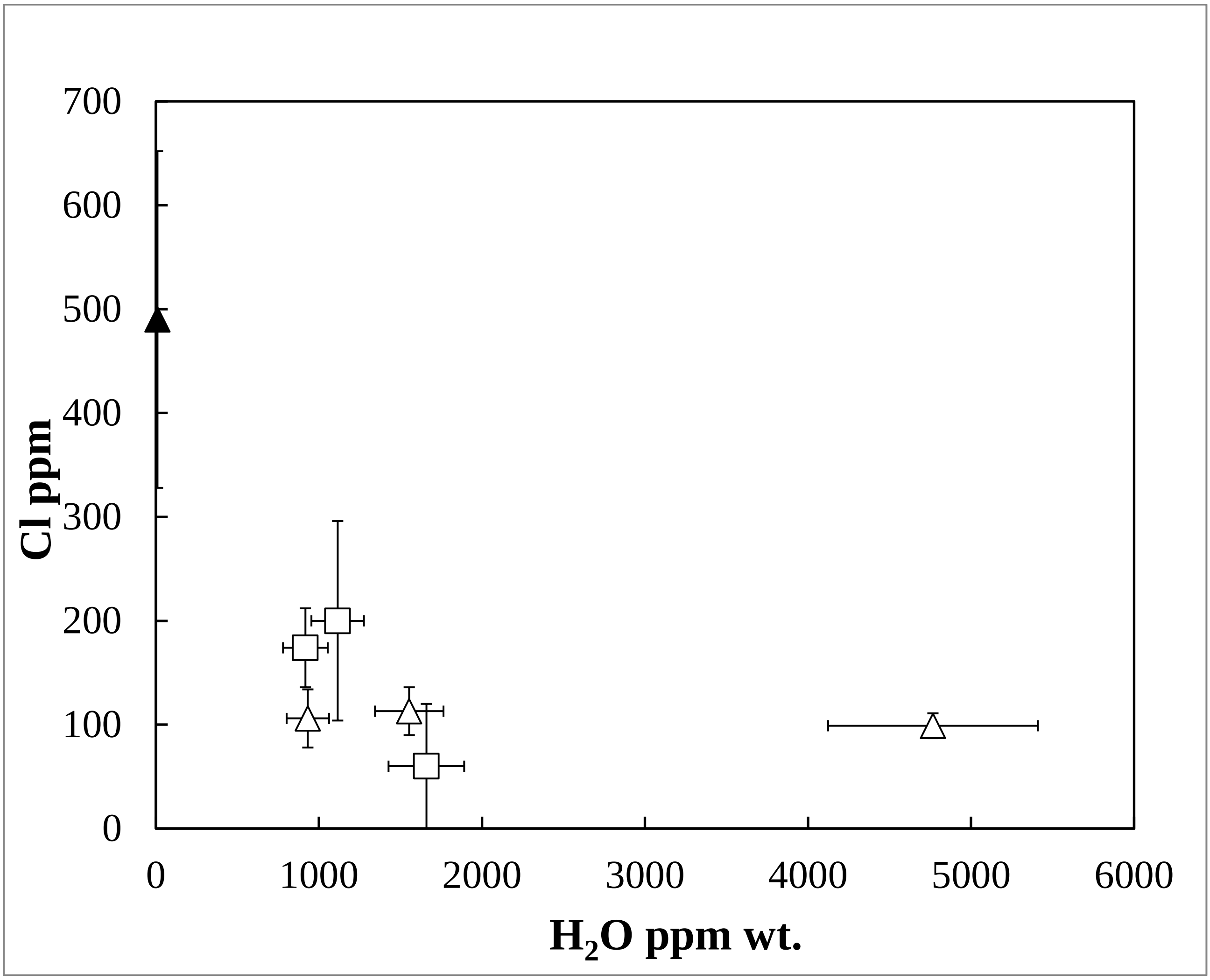
700
600
500
400
300
200
100
0
Cl ppm
0
1000
2000
3000
4000
5000
6000
H2O ppm wt.

Figure 6:

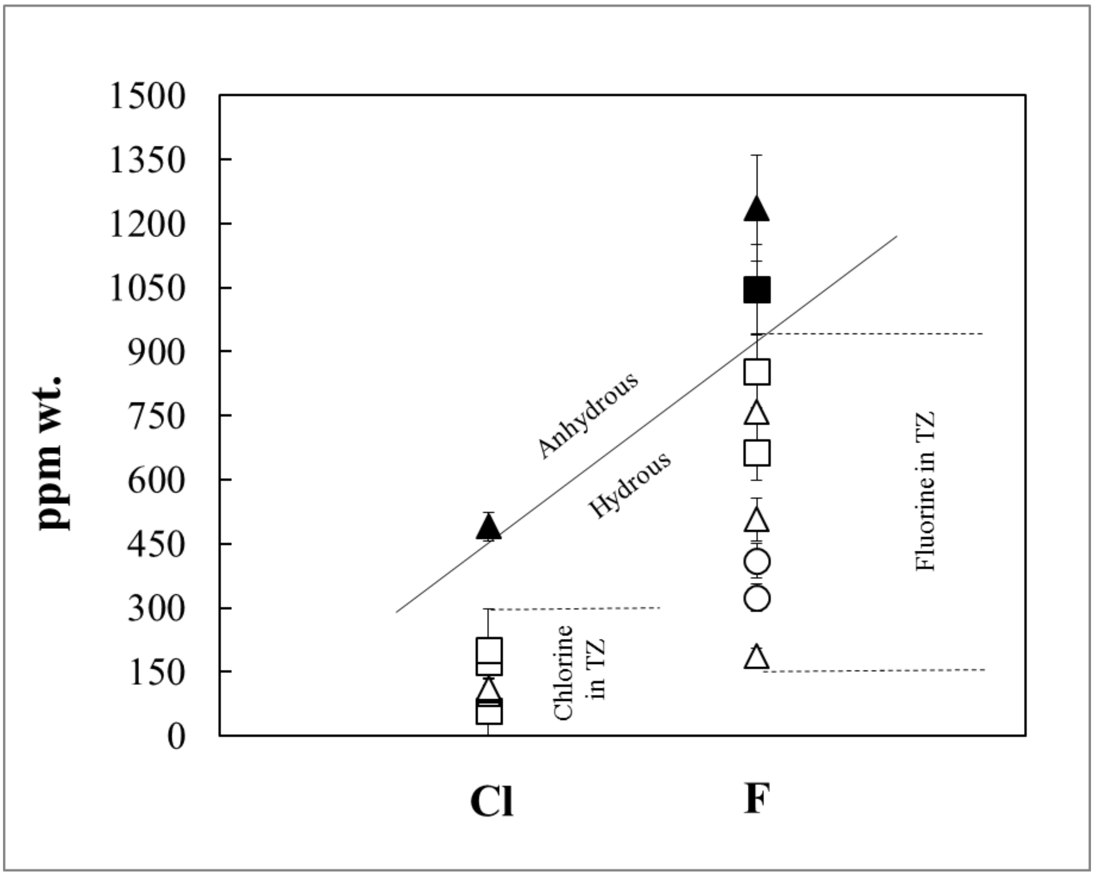

1500
1350
1200
1050
900
750
600
450
300
150
0
ppm wt.
Anhydrous
Hydrous
Fluorine in TZ
Chlorine
in TZ
Cl
F

Figure 7

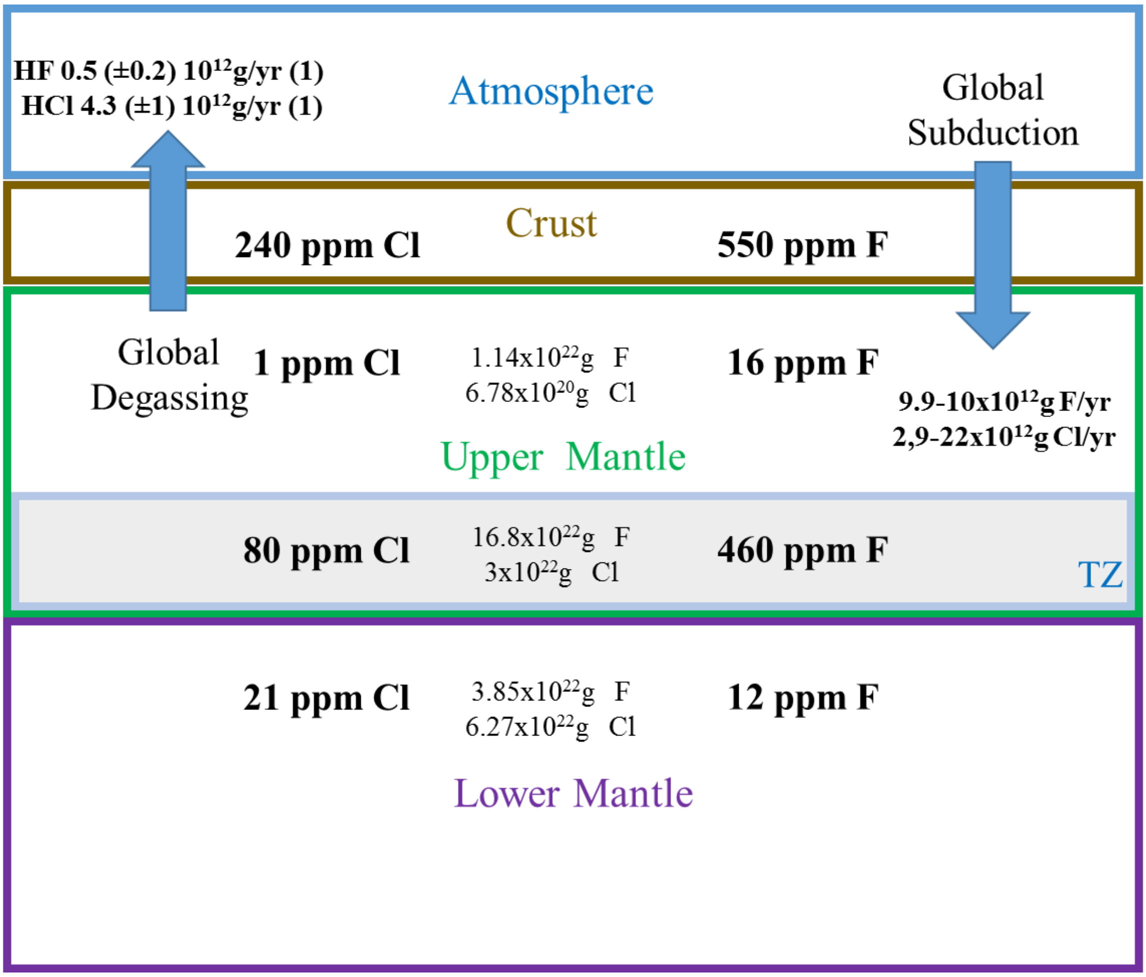
HF 0.5 (±0.2) 10^12g/yr (1)
HCl 4.3 (±1) 10^12g/yr (1)
Atmosphere
Global Subduction
240 ppm Cl
Crust
550 ppm F
Global Degassing
1 ppm Cl
1.14x10^22g F
6.78x10^20g Cl
16 ppm F
9.9-10x10^12g F/yr
2,9-22x10^12g Cl/yr
Upper Mantle
80 ppm Cl
16.8x10^22g F
3x10^22g Cl
460 ppm F
TZ
21 ppm Cl
3.85x10^22g F
6.27x10^22g Cl
12 ppm F
Lower Mantle

Table 1: Starting materials, experimental conditions and sample descriptions.

Sample	P (GPa)	T (°C)	Time (min)	Starting material	Phases
References					
83(*)	15	1400	20	Pure SC	Wadsleyite (>400 µm)
H3698(*)	22	1400	20	Pure SC	Ringwoodite (>400 µm)
Anhydrous					
87_Cl(*)	14	1350	420	SCP + 5wt.% NaCl + 2 wt.% $Mg(OH)_2$	Wadsleyite (20 µm) Enstatite NaCl-glass
S5551(**)	20	1100	240	SCP + 5wt.% NaCl + 2 wt.% $Mg(OH)_2$	Ringwoodite(40 µm) Stishovite (10 µm) NaCl-glass
Hydrous					
40_Cl(*)	14	1100	240	SP + 5wt.% NaCl + 2 wt.% $Mg(OH)_2$	Wadsleyite (40 µm) Enstatite NaCl-glass
86(*)	15	1250	540	SCP + 5wt.% NaCl + 2 wt.% $Mg(OH)_2$	Wadsleyite (30 µm) Enstatite (10 µm) NaCl-glass
88_Cl(*)	14	1400	360	SCP + 5wt.% NaCl + 2 wt.% $Mg(OH)_2$	Wadsleyite (70 µm) Enstatite (10 µm) NaCl-glass
S5553(***)	20	1100	240	SCP + 5wt.% NaCl + 2 wt.% $Mg(OH)_2$	Ringwoodite (>200 µm) stishovite(15 µm) NaCl-glass
H3694(*)	22	1250	240	SCP + 5wt.% NaCl + 2 wt.% $Mg(OH)_2$	Ringwoodite (100 µm) Stishovite (20 µm) NaCl-glass
H3697(*)	22	1400	240	SCP + 5wt.% NaCl + 2 wt.% $Mg(OH)_2$	Ringwoodite (> 300µm) Stishovite (20 µm) NaCl-glass

SC San Carlos olivine, SCP San Carlos olivine powder + SiO_2; SP synthetic powder of SiO_2 + MgO + FeO; (*) Au-Pd capsule, (**) Re capsule, (***) Pt capsule, NaCl pure salt, $Mg(OH)_2$ brucite, Larger grain sizes are given in brackets when measured.

Table 2: Representative analyses of wadsleyites and ringwoodites. Major elements are from EPMA, Cl from PIXE, H_2O from ERDA. Wd= wadsleyite, Rw =ringwoodite, Nb =number of EPMA analysis, Mg#=Mg/(Fe+Mg) ratio atomic, (Fe+Mg)/SiO_2 atomic ratio. Error in brackets is the standard deviation for EPMA analysis and is in (%) for PIXE and ERDA.

Sample	P	T	Time	Phase	Oxydes (%wt)									Nb	Mg#	(Mg+Fe)/Si	(ppm)	
	± 1GPa	±50°C	min		SiO_2	FeO	MnO	Al_2O_3	Na_2O	MgO	CaO	TiO_2	Total				H_2O	Cl
Reference																		
83	15	1400	20	Wd	41.55	9.21	0.12	0.11	0.02	48.48	0.02	0.01	99.63	9	0.90	1.92		
					(0.09)	(0.10)	(0.04)	(0.02)	(0.02)	(0.29)	(0.03)	(0.01)	(0.38)					
H3698	22	1400	20	Rw	41.50	9.70	0.12	0.04	0.01	48.79	0.07	0.01	100.39	14	0.90	1.95		
					(0.31)	(0.14)	(0.05)	(0.04)	(0.01)	(0.27)	(0.02)	(0.02)	(0.38)					
Anhydrous																		
87_Cl	14	1350	420	Wd	41.38	8.56	0.08	0.07	0.16	48.87	0.03	0.03	99.18	7	0.91	1.93		ND
					(0.39)	(0.16)	(0.03)	(0.02)	(0.03)	(0.42)	(0.03)	(0.02)	(0.21)					
S5551	20	1100	240	Rw	41.40	9.00	0.14	0.05	0.06	47.84	0.04	0.01	98.54	4	0.90	1.91		490
					(0.86)	(0.33)	(0.04)	(0.03)	(0.04)	(0.93)	(0.01)	(0.01)	(0.29)					(33)
Hydrous																		
40_Cl	14	1100	240	Wd	41.13	8.84	0.02	0.24	0.22	49.09	0.02	0.02	99.58	6	0.91	1.96	917	174
					(0.34)	(0.20)	(0.02)	(0.04)	(0.05)	(0.52)	(0.01)	(0.03)	(0.75)				(15)	(22)
86	15	1250	540	Wd	41.49	8.57	0.09	0.08	0.19	48.88	0.00	0.02	99.32	6	0.91	1.93	1659	60
					(0.46)	(0.13)	(0.03)	(0.01)	(0.03)	(0.34)	(0.00)	(0.02)	(0.47)				(14)	(60)
88_Cl	14	1400	360	Wd	41.55	8.04	0.05	0.09	0.19	49.65	0.01	0.02	99.6	6	0.92	1.94	1115	200
					(0.20)	(0.20)	(0.03)	(0.02)	(0.02)	(0.24)	(0.01)	(0.02)	(0.35)				(14)	(48)
S5553	20	1100	240	Rw	41.63	7.63	0.07	0.03	0.04	49.42	0.00	0.02	98.84	3	0.92	1.92	4766	99
					(0.22)	(0.13)	(0.03)	(0.02)	(0.01)	(0.04)	(0.00)	(0.02)	(0.42)				(13)	(12)
H3694	22	1250	240	Rw	40.49	7.67	0.04	0.07	0.09	49.97	0.00	0.03	98.36	3	0.92	2.00	932	106
					(0.55)	(0.07)	(0.04)	(0.00)	(0.04)	(0.42)	(0.01)	(0.02)	(0.30)				(14)	(26)
H3697	22	1400	240	Rw	41.37	8.18	0.07	0.06	0.10	49.57	0.01	0.02	99.38	7	0.92	1.95	1554	113
					(0.37)	(0.34)	(0.02)	(0.02)	(0.05)	(0.35)	(0.01)	(0.02)	(0.29)				(13)	(20)

731